

Applying Physics-Informed Enhanced Super-Resolution Generative Adversarial Networks to Finite-Rate-Chemistry Flows and Predicting Lean Premixed Gas Turbine Combustors

Mathis Bode^{a,b,*}

^aJülich Supercomputing Centre, Forschungszentrum Jülich GmbH, 52425 Jülich, Germany

^bFakultät für Maschinenwesen, RWTH Aachen University, Templergraben 64, 52056 Aachen, Germany

Abstract

The accurate prediction of small scales in underresolved flows is still one of the main challenges in predictive simulations of complex configurations. Over the last few years, data-driven modeling has become popular in many fields as large, often extensively labeled datasets are now available and training of large neural networks has become possible on graphics processing units (GPUs) that speed up the learning process tremendously. In fact, the successful application of deep neural networks in fluid dynamics, such as for underresolved reactive flows, is still challenging. This work advances the recently introduced PIESRGAN to reactive finite-rate-chemistry flows. However, since combustion chemistry typically acts on the smallest scales, the original approach needs to be extended. Therefore, the modeling approach of PIESRGAN is modified to accurately account for the challenges in the context of laminar finite-rate-chemistry flows. The modified PIESRGAN-based model gives good agreement in a priori and a posteriori tests in a laminar lean premixed combustion setup. Furthermore, a reduced PIESRGAN-based model is presented that solves only the major species on a reconstructed field and employs PIESRGAN lookup for the remaining species, utilizing staggering in time. The advantages of the discriminator-supported training are shown, and the usability of the new model demonstrated in the context of a model gas turbine combustor.

Keywords: Generative Adversarial Network, Direct Numerical Simulation, Large-Eddy Simulation, Lean Premixed Combustion, Gas Turbine

1. Introduction

Data-driven methods have evolved as important tools in many applications. With the growth in availability and size of often extensively labeled datasets, data-driven models have potential to become more and more accurate. Recently, significant advances in terms of functionality and processing with optimized graphics processing units (GPUs), such as continuously updating network weights in a data-fed training process to minimize loss functions by machine learning (ML) and deep learning (DL), have been made. Examples for successful applications cover a broad range including image processing [1, 2], speech recognition [3], acceleration of drug developments [4], and learning of optimal complex control [5]. Some of these examples employ generative adversarial networks (GANs) [6] and demonstrate that GANs are one powerful way to use DL. A GAN consists of two DL networks: a generator network, which is finally used for data generation, and a discriminator network supporting the training process by assessing if data is real or generated by the generator. As the generator attempts to "fool" the discriminator and the discriminator becomes better and better in discrimination of real and generated data with increasing training time, the overall quality of the generated data improves. Both parts can be independently updated during the training

process and are coupled by the adversarial loss term. By design, GANs learn unsupervised from unlabeled data, which is a significant advantage for many physical applications, for which available training data is often sparse and does not cover the entire target parameter space of interest.

Many recent applications of data-driven models can also be found in the field of fluid dynamics, such as the usage in simulations requiring modeling of the small scales, in particular Reynolds-averaged Navier-Stokes (RANS) simulations and large-eddy simulations (LESs) [7, 8, 9, 10, 11, 12, 13, 14]. This includes the idea of physics-informed networks [15], which has recently emerged. Physics-informed networks employ architectures or loss functions that are designed to support known properties of the underlying physical problems to regularize the learning procedure. Kutz [16] summarized more applications of ML/DL in the field of fluid mechanics.

Bode et al. [17, 18, 19] introduced physics-informed enhanced super-resolution generative adversarial networks (PIESRGANs) as subfilter closure for LES. They advanced ESRGANs (enhanced super-resolution GANs), which were originally developed for two-dimensional (2-D) image super-resolution [20], to handle 3-D physical data and combined it with physical information during the training process. The general training procedure of this network relies on high-fidelity data ("H"), e. g., from a fully resolved direct numerical simulation (DNS), which are filtered ("F") as part of training. The combination of fully resolved data Φ_H and filtered data Φ_F is

*Corresponding author

Email address: m.bode@itv.rwth-aachen.de (Mathis Bode)

used to train the full network with the goal to be able to achieve as accurate as possible reconstructed data ("R") Φ_R with the filtered data as input, which can be used to close any required subfilter terms. It was shown that PIESRGAN gives very good results for LES of turbulence [18, 21, 22] and of spray combustion based on the multiple representative interactive flamelet model (MRIF) [18, 23] if it is used for modeling the unclosed velocity and scalar mixing terms in the filtered Navier-Stokes equations. However, PIESRGAN has not been applied to obtain the filtered chemical source terms directly, which is done in this work for the first time on the example of laminar lean premixed combustion. Even though LES is not necessary in this case due to the lack of turbulence, the challenge to accurately predict small scales from filtered fields remains comparable, as the prediction of flame dynamics and pollutant formation requires fine grids even in the case of laminar flows.

Power plants with gas turbines are an important pillar for combating climate change, as they combine multiple advantages. They have low start-up times and can quickly follow the load demand, balancing the volatility of wind and solar power generation. The investment costs are relatively low, which is important for peaker or backup plants which are only operated for a low number of hours per year. And finally, natural gas is a much cleaner power source than coal, with an easy pathway to incorporate renewable hydrogen or e-methane in the future. One important challenge in the development of advanced highly efficient gas turbine combustors is the minimization of CO emissions under low part load conditions. In particular, interaction between flames and cold secondary air from unfired stages or combustor cooling can lead to perturbations of the oxidation layer in premixed flames resulting in incomplete CO burnout. Modeling of such interaction is often difficult with classical combustion models such as flamelet models, or very expensive when finite rate chemistry is applied. Thus, this physical problem appears to be a good application for advanced, data-driven models such as PIESRGAN.

In this work, a simplified laminar lean premixed model configuration, representing the underlying physical processes described above, is chosen as a first target case for the development of PIESRGAN for reactive finite-rate-chemistry flows. As the scope of this work is on modeling finite-rate-chemistry flows with PIESRGAN, the momentum fields are still computed on DNS resolution, and the full integration in PIESRGAN is left for future work.

2. Case setup of simplified lean premixed combustion

To investigate combustion in stationary gas turbines, Lücknerath et al. [24] developed a test rig with staged combustors. Their configuration features 8 circumferentially arranged burners around a central pilot flame and can be run such that not all burners are loaded. Loaded burners then interact with neighboring air jets with the impact on chemistry, especially CO, depending on the mixing velocity. This setup is mimicked with two different cases in this work: a laminar setup and a turbulent setup. All cases in this work used methane as fuel, and a chem-

ical mechanism derived from GRI3.0 [25] by Luca et al. [26] with 16 species and 72 reversible reactions was employed.

A simplified configuration to reproduce the main characteristics of a laminar flame/air jet interaction and the resulting increase of CO was employed in this work. The focus is on one premixed fuel inlet, and the flame is diluted with air by two symmetric side inlets downstream. To keep simulation cost low, this is modeled as a 2-D model domain discretized by a uniform mesh and periodic boundary conditions in the third dimension, and the flame was resolved by 18 grid points per flame thickness, resulting in a $[4096 \times 192]$ mesh. Even though the setup considered here is symmetric, the axis symmetry was not used in the simulations and a domain with two separate inlets was considered to enable the possibility to study unsymmetric configurations with more complex dilution patterns in the future with the same setup. The inlet velocity U_{inlet} was chosen as 3.0 m s^{-1} , the air-fuel equivalence ratio ϕ was set to 0.55, and the inlet velocities of the side inlets V_{inlet} were varied from 0.0 m s^{-1} (reference case without dilution) to 8.0 m s^{-1} . For training the network, the cases with $V_{\text{inlet}} = 0.0 \text{ m s}^{-1}$ and $V_{\text{inlet}} = 4.0 \text{ m s}^{-1}$ were used, which are also illustrated in Fig. 1 with their respective mixture fraction fields Z , CO mass fraction fields Y_{CO} , axial velocity fields U , and temperature fields T .

This laminar lean premixed combustion application is used as target case for the development of PIESRGAN for reactive finite rate chemistry flows for three reasons. First, the laminar case allows to fully focus on the proper reconstruction of the finite rate chemistry scalar fields without dealing with the issue of turbulent fluctuations. Thus, the velocities were not used for training in this work; however, note that this does not mean that the velocities are not considered by the network. As the chemistry is coupled with the velocities, the effect of different flow velocities and potentially related different strain rates is implicitly recognized by the network by recognizing different scalar field configurations. Second, models for premixed combustion with a focus on emissions at varying mixtures often lack accuracy if the species concentration exceeds its common range at the local mixture. Third, the resulting chemistry of lean premixed combustion cases can be highly non-linear even for relatively simple configurations, making it a very appealing target case for the developed model.

The goal of such a simulation could be to accurately determine CO emissions at different levels of interaction between the flame and the lateral inflow of air. Furthermore, the underlying physical processes leading to different CO levels at the exhaust at varying levels of interaction are interesting. The leading quantity to compare cases has been the average mass flux of CO in the domain. It will be found as part of the variations in the application chapter that CO emissions in the lean yet unperturbed configuration converged quickly to the equilibrium concentration. Mild dilution from the lateral inlet reduces the CO emissions below the unperturbed case, without the configuration reaching its equilibrium concentration. Even stronger dilution with air further reduces the equilibrium concentration, but CO consumption turns out to be very slow, with a virtual freeze of the CO concentration at one point resulting in an overall increase of CO emissions at the outlet. Above-mentioned

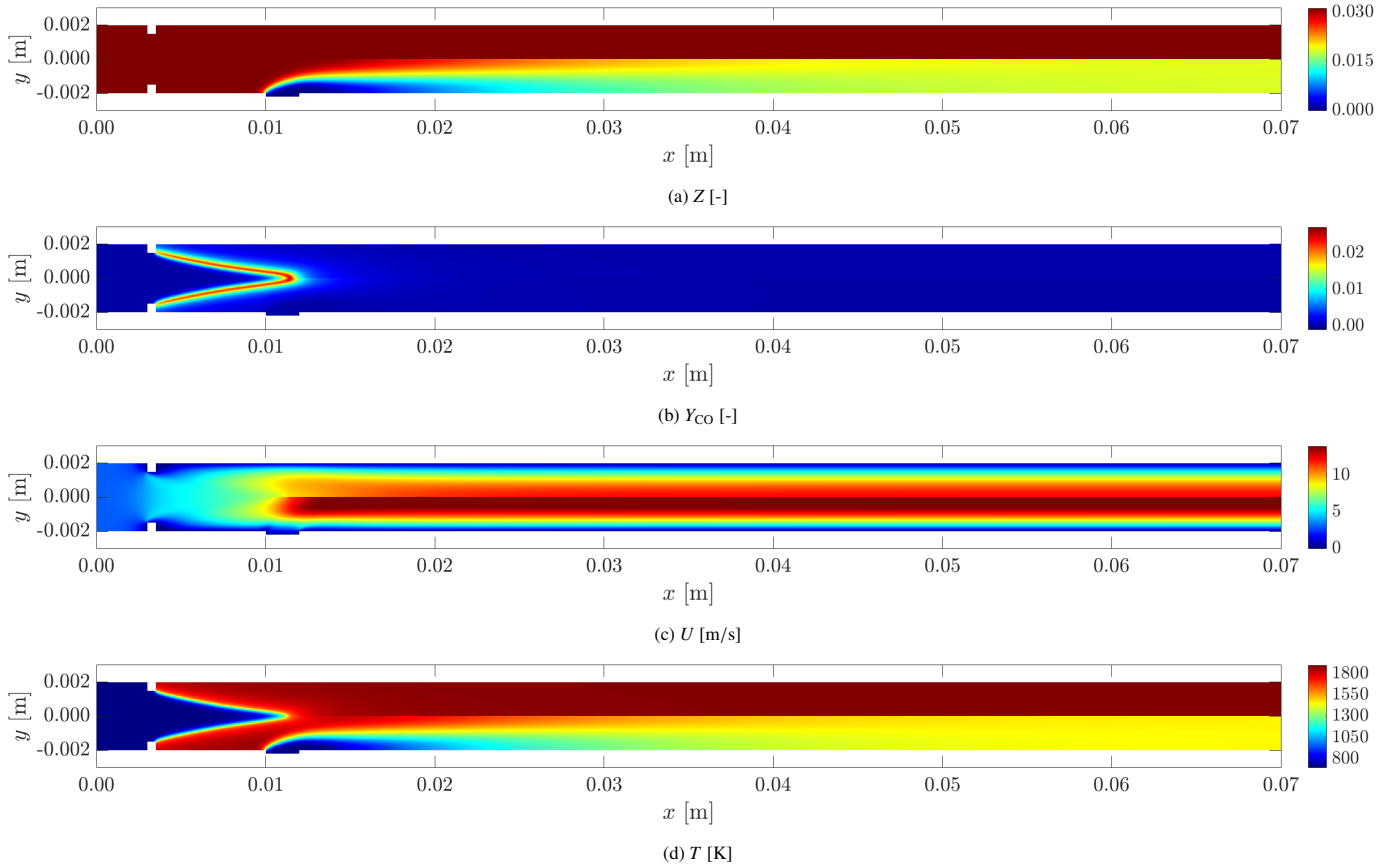


Figure 1: Fully resolved DNS results of the laminar model setup for the mixture fraction, CO mass fraction, axial velocity, temperature for the case with wall, i. e., $V_{\text{inlet}} = 0.0 \text{ m s}^{-1}$, (top) and $V_{\text{inlet}} = 4.0 \text{ m s}^{-1}$ (bottom). Note that not the full length in x -direction is shown.

average mass of CO in the domain will be used as key indicator for the accuracy of the modeling approach introduced here. Furthermore, the full transition phase from the initialization to steady-state is used for training and validation, although the final result is steady-state. This increases the number of learning samples and is also more challenging for the model, as multiple "operating points" are passed during initialization.

3. PIESRGAN

This section describes the PIESRGAN model for finite-rate-chemistry flows. It starts with a summary of PIESRGAN and develops the extensions for finite-rate chemistry afterward step-by-step.

3.1. Base PIESRGAN model

PIESRGAN for turbulence and passive scalar transport was introduced by Bode et al. [18]. The method relies on a GAN, which is trained with "H"/"F" data pairs, and a closure algorithm. The suggested network by Bode et al. [18] is sketched in Fig. 2. The generator heavily uses combinations of leaky rectified linear unit (LeakyReLU) layers for activation [27] and 3-D CNN layers (Conv3D) [28]. Previous architectures relied on the residual block (RB), which contains fundamental architectural elements such as residual dense blocks (RDBs) with

skip-connections. This was extended for ESRGAN to the residual in residual dense block (RRDB) with residual scaling factor β_{RSF} , helping to avoid instabilities in the forward and backward propagation. The RRDB is essential for the performance of state-of-the-art super-resolution. The RDBs use dense connections inside, i. e., the output from each layer within the dense block (DB) is sent to all the following layers. The discriminator mainly employs basic CNN layers (Conv3D) with LeakyReLU layers for activation with and without batch normalization (BN). The final layers combine a dropout with dropout factor β_{dropout} with a fully connected layer and LeakyReLU activation.

As example to summarize the closure algorithm, the transport of a passive specific scalar ϕ over time t in a non-reactive, incompressible flow with constant molecular diffusivity D and without body forces can be described by

$$\partial_t(\phi) + \mathbf{u} \cdot \nabla(\phi) = D\nabla^2(\phi) \quad (1)$$

with bold notation for vectors, ∇ as del operator, corresponding to spatial coordinates, such as $\mathbf{x} = (x_1, x_2, x_3)^T$ for a Cartesian coordinate system or $\mathbf{x} = (r, \theta, \phi)^T$ for a spherical coordinate system, and ∂_t as time derivative.

For LES, an homogeneous filter operation, which moreover is assumed to be a Reynolds operator and denoted with an over-

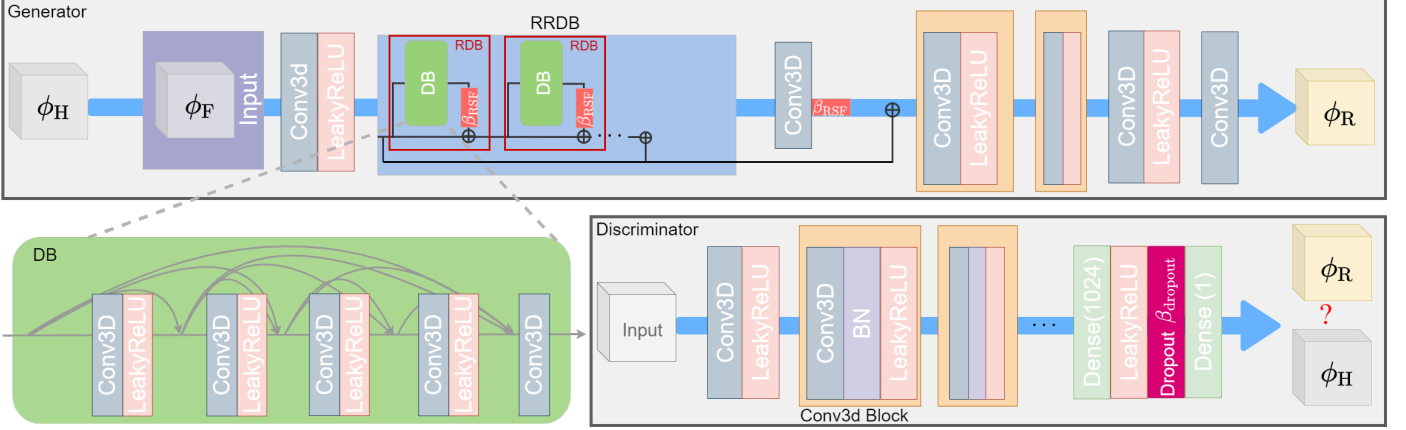


Figure 2: Sketch of PIESRGAN. "H" denotes high-fidelity data, "F" are corresponding filtered data, and "R" are the reconstructed data. The components are: Conv3D - 3-D Convolutional Layer, LeakyReLU - Activation Function, DB - Dense Block, RDB - Residual Dense Block, RRDB - Residual in Residual Dense Block, β_{RSF} - Residual Scaling Factor, BN - Batch Normalization, Dense - Fully Connected Layer, Dropout - Regularization Component, and $\beta_{dropout}$ - Dropout Factor. Image from [18].

bar, and Reynolds splitting as

$$\{\cdot\} = \overline{\{\cdot\}} + \{\cdot\}' \quad (2)$$

with the overbar denoting the filtered part and the prime the subfilter part of a quantity with

$$\overline{\{\cdot\}'} = \overline{\{\cdot\}}' = \overline{\{\cdot\}} \quad (3)$$

and

$$\overline{\{\cdot\}'} = 0 \quad (4)$$

are defined. Introducing Reynolds splitting for \mathbf{u} and ϕ in Eq. (1) and applying the filter operation to all terms, results in the filtered equation solved in LES. This transport equation reads

$$\partial_t(\overline{\phi}) + \overline{\mathbf{u}} \cdot \nabla(\overline{\phi}) = D\nabla^2(\overline{\phi}) - \overline{\mathbf{u}' \cdot \nabla(\phi')}. \quad (5)$$

The last term on the right side is unclosed as it requires subfilter information, which are not solved for in LES. This closure is done with PIESRGAN. If Φ_F^n denotes a discretized filtered solution at time step n , including velocity and all scalar fields, the resulting simulation workflow for closing unclosed terms Ψ_F^n is as follows:

1. Use the PIESRGAN to reconstruct Φ_R^n from Φ_F^n .
2. Use Φ_R^n to estimate the unclosed terms Ψ_F^n by evaluating the local terms with Φ_R^n and applying a filter operator.
3. Use Ψ_F^n and Φ_F^n to advance the filtered equations to Φ_F^{n+1} .

3.2. PIESRGAN for lean premixed combustion

The application of finite rate chemistry usually comes along with the solution of coupled transport equations for the mass fractions Y of every species α . This set of equations reads

$$\partial_t(\rho Y_\alpha) + \nabla \cdot (\rho \mathbf{u} Y_\alpha) = \nabla \cdot (\rho D_\alpha \nabla(Y_\alpha)) + \dot{\omega}_\alpha \quad (6)$$

with $\dot{\omega}_\alpha$ as chemical source term of species α , which can be also written as $\dot{\omega}_\alpha = \rho S_\alpha$. All equations are coupled by the chemical

mechanism, which provides D and $\dot{\omega}_\alpha$ depending on the local composition of all species as well as temperature and pressure.

In contrast to Eq. (1), ρ and D are not constant for reactive flows. Due to the variable density, Favre-filtering is therefore more convenient in these cases compared to the earlier introduced Reynolds-filtering. Favre-filtering is denoted by a tilde and defined as

$$\tilde{\{\cdot\}} = \frac{\overline{\{\rho \cdot\}}}{\overline{\rho}}. \quad (7)$$

The corresponding Favre-decomposition reads

$$\{\cdot\} = \tilde{\{\cdot\}} + \{\cdot\}'''. \quad (8)$$

Note that $\overline{\{\cdot\}'''} \neq 0$ but $\overline{\rho \{\cdot\}'''} = 0$.

Introducing Favre-decomposition in Eq. (6), using the continuity equation, and Reynolds-filtering all terms, leads to the filtered set of equations as

$$\overline{\rho} \partial_t(\tilde{Y}_\alpha) + \overline{\rho \mathbf{u}} \cdot \nabla(\tilde{Y}_\alpha) = \overline{\nabla \cdot (\rho D_\alpha \nabla(Y_\alpha))} - \nabla \cdot (\overline{\rho \mathbf{u} Y_\alpha}''') + \overline{\rho S_\alpha}. \quad (9)$$

Note that all terms on the right side are unclosed. While the second term on the right side, the turbulent transport, is similar to the unclosed term in Eq. (5), the last term, the averaged source term, and the first term, the molecular transport, which is unclosed due to the non-constant diffusion coefficients and the variable density, are new. However, also the new unclosed terms can be closed on the reconstructed fields, however, not as simple as the turbulence term as outlined in this work.

Two important challenges in this context should be highlighted. First, the chemical source terms are often only active in a very fine zone, acting on the smallest scales. This makes it very challenging to accurately model their impact in filtered equations. Second, diffusion models, such as the Curtiss-Hirschfelder approximation [29], are often very complex and further effects, such as preferential diffusion, exacerbate the situation even further.

3.3. Full PIESRGAN model

The target case in this study is laminar, and thus an LES is not necessary for predicting the velocity field. However, filtered equations are still used to model the effect of an underresolved flow field on chemistry. The effect of such underresolved species fields, as would be commonly encountered in LES or RANS simulation of more complex setups, can be clearly seen in Fig. 4, where the domain-averaged mass of CO deviates by 19 % from the fine DNS grid to the coarser underresolved grid. To keep things simple, a box filter is employed for all fields but the model closure is only used for the scalar fields. Due to the complexity on the finest scales, which need to be reconstructed and the complex physical processes there, a straight-forward usage of the approach by Bode et al. [18] was not successful, resulting in significant deviations in a priori tests and divergence in a posteriori scenarios. As a result, a modified way, in which the full transport equations are solved on the reconstructed grid, is pursued here, retaining the complex direct interaction of transport and chemical source terms. The resulting model can be seen as solving the governing equations on multiple grids, utilizing the super-resolution capabilities of PIESRGAN to achieve the necessary resolution for accurate chemistry computations while solving the overall flow field on a much coarser mesh after mapping the solution back. The algorithm starts with the filtered solution Φ_F^n at time step n , which includes the entirety of all relevant fields in the simulation, and consists of repeating the following steps:

1. Use the PIESRGAN to reconstruct Φ_R^n from Φ_F^n .
2. Use Φ_R^n to update the chemistry to $\Phi_R^{n:\text{update}}$ by solving the unfiltered transport equations (Eq. (1)) on the mesh of Φ_R^n .
3. Use $\Phi_R^{n:\text{update}}$ to estimate the unclosed terms Ψ_F^n in the filtered transport equations of Φ by evaluating the local terms with $\Phi_R^{n:\text{update}}$ and applying a filter operator.
4. Use Ψ_F^n and Φ_F^n to advance the filtered transport equations of Φ to Φ_F^{n+1} .

Within this algorithm, the chemistry source terms on the resolved field $\Phi_R^{n:\text{update}}$ in step 2 can be evaluated by multiple methods, such as tabulated flamelet and finite-rate-chemistry approaches. All approaches benefit from the locally high resolution on the reconstructed mesh. As in other simulations, flamelet approaches might lack accuracy due to their low-dimensional mapping of the thermochemical parameter space, and finite-rate-chemistry techniques can be expected to give more reliable results. Therefore, this work focuses on finite-rate chemistry in the following. However, using tabulated flamelet models might enable even further computing cost reductions for more complex cases.

3.4. Implementation details

As the PIESRGAN is applied to the species fields instead of the velocity field as in [18], the continuity loss term, which was used previously to enforce the continuity equation, is replaced by a physically motivated term enforcing all species to sum up to one, i. e., $\sum_i Y_i = 1$. This condition can also be enforced by computing one mass fraction as one minus the sum of all

others, as it is often done in simulations, however, this approach gave worse results in tests in the context of PIESRGAN and was therefore dropped.

With the new term for species conservation, $\beta_4 L_{\text{species}}$, the used loss function reads

$$\mathcal{L} = \beta_1 L_{\text{adv.}} + \beta_2 L_{\text{pixel}} + \beta_3 L_{\text{gradient}} + \beta_4 L_{\text{species}}, \quad (10)$$

where $\beta_1, \beta_2, \beta_3$, and β_4 are coefficients weighting the different loss term contributions; in this work, these coefficients were always equally scaled such that the sum of all non-zero weighting coefficients remained equal to one. Note that all loss terms are non-dimensional, since all operators and input fields used are non-dimensionalized. $L_{\text{adversarial}}$ is the discriminator/generator relativistic adversarial loss [1], which reflects both how well the generator is able to generate high-resolution turbulence samples that look like real, DNS-obtained fully resolved scalar fields, and how well the discriminator is able to distinguish between real and generated data. The pixel loss L_{pixel} and the gradient loss L_{gradient} are defined as the mean-squared error (MSE) of the quantity itself and of the gradient of the quantity, respectively [17]. Note that an element conservation term was also elaborated during model development. For the here considered cases, this additional term showed negligible impact on the results and was thus dropped.

Filter type and filter width are also critical implementation details. Bode et al. [18] pointed out that PIESRGAN-LES is very robust with respect to the filter width. Bode [30] demonstrated how multiple filter widths can be considered during training to achieve flexibility with respect to training mesh size and local filter width. All common filter types can be generally employed with PIESRGAN.

Bode et al. [18] emphasized the importance of proper normalization of input quantities. For the mass fraction fields this was not necessary, as they are non-dimensional by nature. However, other quantities, such as the density, were scaled between zero and one for training and retrieval. Furthermore, it was tried to improve the accuracy by logarithmic scaling of the mass fraction fields to account for their different orders of magnitudes. This did not give a reasonable improvement and therefore was not further pursued. The numerical solver and hyperparameters, such as network parameters learning rates for the generator training and discriminator training, $l_{\text{generator}}$ and $l_{\text{discriminator}}$, were chosen similarly as by Bode et al. [18] and are also summarized in Table 1.

3.5. Reduced PIESRGAN model

The algorithm introduced in Sec. 3.3 raises the question, why the equations are not directly solved on the finer mesh, omitting the costly reconstruction step. In fact, the previously described "full" PIESRGAN model should be seen as idealized proof of concept, establishing that arbitrary super-resolution of reactive flow fields between meshes is possible and yields satisfactory results. To actually achieve a speed-up compared to a conventional, fully resolved simulation, additional modeling steps are necessary. Some possibilities for this are discussed in the following.

Table 1: Overview of the PIESRGAN hyperparameters. The given ranges represent the sensitivity intervals with acceptable network results. The central values were finally used in this work. Note that the given boundaries are not combined sets of hyperparameters and therefore do not sum up to one.

| | |
|----------------------------|--|
| β_1 | $[0.2 \times 10^{-5}, 0.6 \times 10^{-4}, 0.8 \times 10^{-4}]$ |
| β_2 | $[0.793\ 27, 0.869\ 94, 0.918\ 12]$ |
| β_3 | $[0.04, 0.06, 0.15]$ |
| β_4 | $[0.01, 0.07, 0.08]$ |
| β_{RSF} | $[0.1, 0.2, 0.3]$ |
| β_{dropout} | $[0.2, 0.4, 0.5]$ |
| $l_{\text{generator}}$ | $[1.2 \times 10^{-6}, 4.5 \times 10^{-6}, 5.0 \times 10^{-6}]$ |
| $l_{\text{discriminator}}$ | $[4.4 \times 10^{-6}, 4.5 \times 10^{-6}, 8.5 \times 10^{-6}]$ |

A first trivial optimization is to only reconstruct the fine mesh in cells which are expected to feature high mass fraction gradients, i. e., in the vicinity of the flame front. This can be simply tracked by, e. g., the progress variable gradient and already reduces the overall cost significantly. The resulting model can then be considered as a form of highly flexible, local and temporal adaptive mesh refinement - which can also be applied on structured grids, where such local refinement otherwise requires complex methods such as overset grids. An issue that remains is that the computational effort for the reconstruction of species scales quadratically with the number of simultaneously reconstructed quantities. Even if only performed locally on parts of the mesh, this can quickly become technically challenging even on modern GPUs, if large chemical reaction mechanisms are employed. To counteract this effect, a second optimization to significantly reduce the number of reconstructed species has been developed. For that, the species are split into primary species ("p") and secondary species ("s"). The fine-scale equations are only solved for the primary species while the chemistry evolution of the secondary species is directly predicted by the network based on all other species. This can be seen as a chemtable lookup utilizing the entire chemical space instead of a low-dimensional mapping of it as in traditional chemtable models. It was found that the overall performance of this model and especially the prediction of the evolution of the secondary species can be significantly improved by introducing time staggering for primary and secondary species. Thus, for the presented results with the reduced PIESRGAN model, also denoted PIESRGAN_S, the velocities were updated in the same time step as the secondary species, while the update of the primary species was shifted by half a time step. More precisely, the lookup of the secondary species $Y_{s,i}^{n+1}$ at time $t + 1$ by means of PIESRGAN was done with the input quantities $Y_{s,i}^n$ and $Y_{p,i}^{n+1/2}$, representing the full thermochemical state space as temperature and density are implicitly included for the case without heat losses considered.

As the full PIESRGAN is a full representation of the reduced version PIESRGAN_S, it can be used to systematically identify primary and secondary quantities employing AutoML [31]. Simply put, the AutoML algorithm systematically checks the sensitivity of changes to the primary and secondary species set to find reduced versions with sufficient accuracy. The full PIESRGAN acts as the optimal solution within this optimization

and therefore helps with faster convergence. Technically, the optimization of the species set is treated as a hyperparameter optimization, and consequently three new hyperparameters were introduced. First, two new hyperparameters describing the primary and secondary species set, β_p and β_s , with each element being either zero or one and the boundary condition

$$(\beta_p + \beta_s) \cdot (\beta_p + \beta_s) = n_{\text{species}}. \quad (11)$$

Here, n_{species} is the number of species in the mechanism, which is 16 for the considered case. Furthermore, the loss function during the AutoML procedure is extended by another term with hyperparameter β_5 resulting in

$$\mathcal{L} = \beta_1 L_{\text{adv.}} + \beta_2 L_{\text{pixel}} + \beta_3 L_{\text{gradient}} + \beta_4 L_{\text{species}} + \beta_5 L_{\text{time}}. \quad (12)$$

The new term $\beta_5 L_{\text{time}}$ measures "a posteriori" accuracy by considering the MSE for multiple successive time steps compared to the result achieved with the full PIESRGAN. This term can become very expensive. Therefore, it was evaluated on a very small toy problem with 32^3 cells instead of the full domain. Five time steps with fixed time step size were considered, and β_5 was chosen of the order of β_4 while reducing β_2 to remain at $\sum_i \beta_i = 1$.

Overall, the procedure to run efficient PIESRGAN-LES can be summarized by the following steps:

1. Run suitable DNSs to generate a database Φ_H .
2. Compute Φ_H/Φ_F data pairs for the training of the network.
3. Train the full PIESRGAN.
4. Optimize the full PIESRGAN to a reduced PIESRGAN using AutoML.
5. Use the reduced PIESRGAN to study the target problem with PIESRGAN-LES.

For the present case, the set of CH₄, CO, OH, and CO₂ as primary species was found to give very good results. This is interesting for multiple reasons. First, neither H₂O nor H^o/H₂ are included in the set of primary species, even though they are known to be important for methane oxidation as product of the complete oxidation and in crucial elementary reactions, such as CH₄ + H^o → CH₃ + H₂ and H^o + O₂ → OH^o + O^o, respectively. Second, it emphasizes the importance of the CO consumption elementary reaction, CO + OH^o → CO₂ + H^o, which is the key reaction affecting CO emissions in the post flame region. Note that the sets of primary and secondary species do not indicate which species are physically the most relevant. Instead, these sets quantify the level of accuracy to which a species needs to be known during a simulation.

3.6. A priori testing

The accuracy of the PIESRGAN model for lean premixed combustion super-resolution is first evaluated based on an a priori test for the full model (denoted "R") and the reduced PIESRGAN, PIESRGAN_S (denoted "RS"). For that, the networks were trained with the $V_{\text{inlet}} = 0.0 \text{ m s}^{-1}$ and $V_{\text{inlet}} = 4.0 \text{ m s}^{-1}$ case data and applied to reconstruct fields of the $V_{\text{inlet}} = 2.0 \text{ m s}^{-1}$ case containing the reaction zone. The results are shown in Fig. 3. The visual agreement between fully

resolved data and reconstructed data is very good. The filtered data clearly lack resolution around the reaction zone, and it cannot be expected that it is possible to accurately advance the filtered fields without an advanced closure model. The agreement between the full and reduced PIESRGAN model is also striking, suggesting that the combination of super-resolved full transport equations for some important species with a pre-computed network look-up for other species is a promising approach. Note that only the CO mass fraction field was directly reconstructed by the PIESRGAN-networks. Temperature and mixture fraction are computed from all reconstructed mass fraction fields and are only shown for demonstration purposes here.

3.7. *A posteriori testing*

For a posteriori testing, the $V_{\text{inlet}} = 2.0 \text{ m s}^{-1}$ case was recomputed on an eight times coarser mesh in each non-periodic direction using PIESRGAN and PIESRGAN_S closures. All cases were initialized with a 1-D flamelet solution and zero initial velocity. In Fig. 4, the domain-averaged CO mass (m_{CO}) over time is shown for the fully resolved DNS case, the PIESRGAN case, and an underresolved case without closure. The agreement between the fully resolved case and PIESRGAN is very good for all time steps. The underresolved case features a smaller increase of CO mass in the beginning and is not able to accurately predict CO consumption towards steady-state. Also in this a posteriori test, the reduced PIESRGAN model delivers results extremely close to the full model.

3.8. *Generality*

The a posteriori test showed that it is possible to accurately predict the $V_{\text{inlet}} = 2.0 \text{ m s}^{-1}$ case with a network trained with $V_{\text{inlet}} = 0.0 \text{ m s}^{-1}$ and $V_{\text{inlet}} = 4.0 \text{ m s}^{-1}$ case data. This was a classical "interpolation" case. However, an important question is how general the model is and whether the network has certain "extrapolation" abilities, i. e., can predict a case outside of the training range. For this, the $V_{\text{inlet}} = 8.0 \text{ m s}^{-1}$ case is rerun on a coarser mesh. This case features higher velocities and consecutive strain rates, which - as explained earlier - implicitly effect also the chemistry fields and were not seen during training. The results are presented in Fig. 5 for the average CO mass in the domain. As before, the agreement between the fully resolved case and PIESRGAN is very good.

Besides the fully resolved result and the PIESRGAN result, a result for a network trained without the discriminator part (denoted "CNN") is given in Fig. 5. The CNN case overpredicts the steady-state amount of CO mass after successfully predicting the evolution in the beginning. A detailed comparison of the PIESRGAN and CNN results reveals that the CNN has problems predicting the reactions in high velocity areas, similar to an underresolved simulation, while the PIESRGAN gives much better results there. This emphasizes the better extrapolation capabilities of GANs compared to simpler networks and is an important result. Note that this advantage is paid for by higher training cost and typically more convergence issues during training.

4. Conclusions

This work advances the PIESRGAN-based modeling approach to reactive finite-rate-chemistry flows. It is shown how a newly devised model, combining super-resolution with direct network lookup for chemistry computation, can be used to accurately predict the evolution of a laminar lean premixed reactive flow on a coarser filtered mesh. For that, the modeling algorithm and loss function of PIESRGAN were modified. To enable practical usage of this model, a staggered splitting in primary and secondary species is introduced, which significantly reduces computational cost and simplifies the application on current GPUs, while maintaining the accuracy almost completely.

Although a speedup was measured for the 2-D laminar target case, the usage of the model for this case seems questionable, as the DNS is cheap and fast enough to run fully resolved simulations. However, for larger 3-D laminar cases and especially for turbulent setups, this is not possible and the here developed methods, such as the splitting, allow for a significant increase in simulation speed and thus enable parameter variations, such as complex geometry and green fuels variations. Overall, the developed approach allows for a significantly faster development of the next generation of energy devices, such as turbines with hydrogen and engines with ammonia as fuel.

The full integration of chemistry and turbulence in one PIESRGAN is demonstrated in a follow-up paper focusing on PIESRGAN for turbulent premixed flame kernels [32].

Acknowledgements

The author acknowledges computing time grants for the projects JHPC55 and TurbulenceSL by the JARA-HPC Vergabegremium provided on the JARA-HPC Partition part of the supercomputer JURECA at Jülich Supercomputing Centre, Forschungszentrum Jülich, the Gauss Centre for Supercomputing e.V. (www.gauss-centre.eu) for funding this project by providing computing time on the GCS Supercomputer JUWELS at Jülich Supercomputing Centre (JSC), and funding from the European Union's Horizon 2020 research and innovation program under the Center of Excellence in Combustion (CoEC) project, grant agreement no. 952181.

References

- [1] X. Wang, K. Yu, S. Wu, J. Gu, Y. Liu, C. Dong, Y. Qiao, C. Loy, ES-RGAN: Enhanced Super-Resolution Generative Adversarial Networks, Lecture Notes in Computer Science 11133 (2019) 63–79.
- [2] H. Greenspan, B. Van Ginneken, R. M. Summers, Guest editorial deep learning in medical imaging: Overview and future promise of an exciting new technique, IEEE Transactions on Medical Imaging 35 (5) (2016) 1153–1159.
- [3] G. Hinton, L. Deng, D. Yu, G. Dahl, A.-r. Mohamed, N. Jaitly, A. Senior, V. Vanhoucke, P. Nguyen, B. Kingsbury, et al., Deep neural networks for acoustic modeling in speech recognition, IEEE Signal processing magazine 29 (2012).
- [4] A. Bhati, S. Wan, D. Alfe, A. Clyde, et al., Pandemic drugs at pandemic speed: infrastructure for accelerating COVID-19 drug discovery with hybrid machine learning- and physics-based simulations on high performance computers, Interface Focus 20210018 (2021).

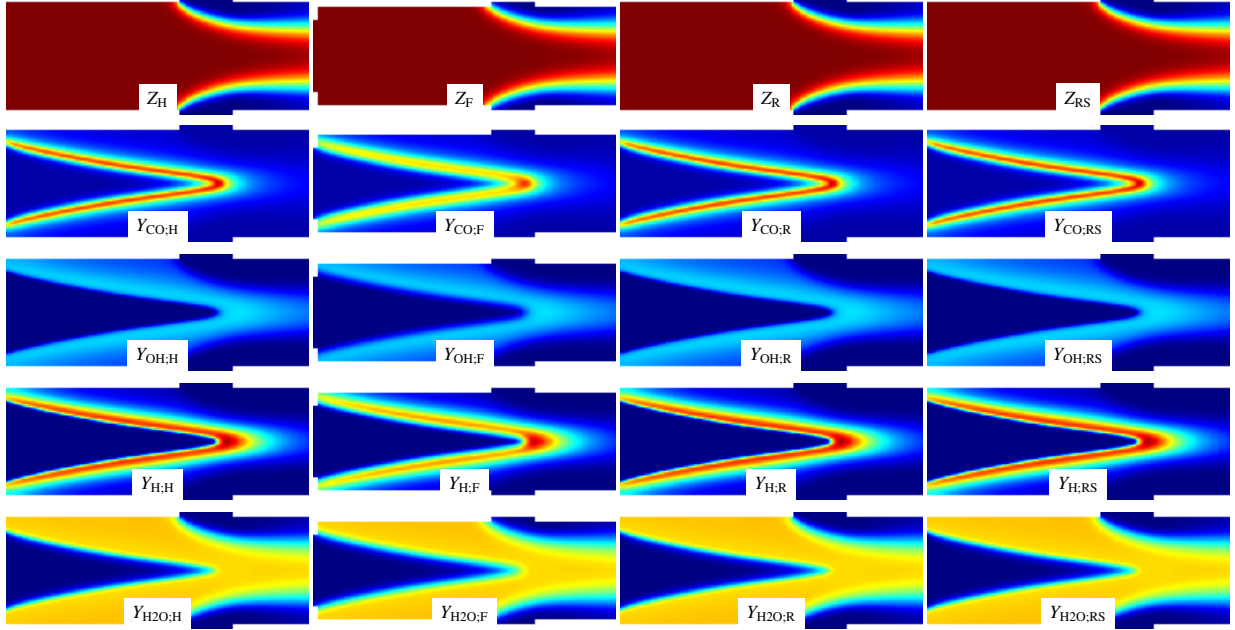


Figure 3: Visualization of DNS (first column), filtered (second column), and reconstructed fields for the $V_{\text{inlet}} = 2.0 \text{ m s}^{-1}$ case employing PIESRGAN (third column) and PIESRGAN_S (fourth column). Results for mixture fraction, CO mass fraction (primary species), OH mass fraction (primary species), H^o mass fraction (secondary species), and H₂O mass fraction (secondary species) are shown.

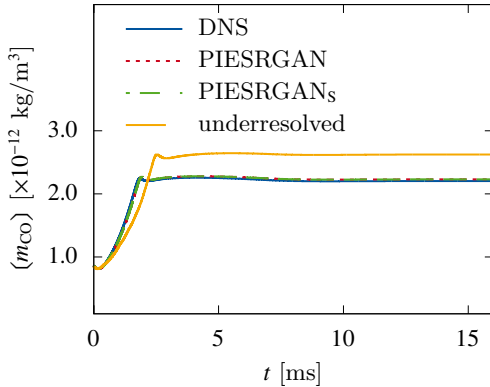


Figure 4: Plot of the domain-averaged CO mass over time for a fully resolved case, a full PIESRGAN case, a reduced PIESRGAN case, and an underresolved case without closure for the $V_{\text{inlet}} = 2.0 \text{ m s}^{-1}$ case.

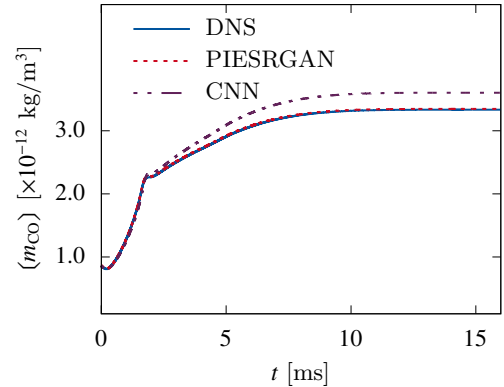


Figure 5: Plot of the domain-averaged CO mass over time for a fully resolved case, a PIESRGAN case, and CNN case for the $V_{\text{inlet}} = 8.0 \text{ m s}^{-1}$ case. Note that the reduced PIESRGAN gave very similar results to the full PIESRGAN and was therefore skipped in this plot.

[5] O. Vinyals, I. Babuschkin, W. Czarnecki, M. Mathieu, A. Dudzik, J. Chung, et al., Grandmaster level in StarCraft II using multi-agent reinforcement learning, *Nature* 575 (2019) 350–354.

[6] I. Goodfellow, J. Pouget-Abadie, M. Mirza, B. Xu, D. Warde-Farley, S. Ozair, A. Courville, Y. Bengio, Generative adversarial nets, in: *Advances in neural information processing systems*, 2014, pp. 2672–2680.

[7] M. Ihme, C. Schmitt, H. Pitsch, Optimal artificial neural networks and tabulation methods for chemistry representation in les of a bluff-body swirl-stabilized flame, *Proceedings of the Combustion Institute* 32 (2009) 1527–1535.

[8] R. Maulik, O. San, A neural network approach for the blind deconvolution of turbulent flows, *Journal of Fluid Mechanics* 831 (2017) 151–181.

[9] M. Bode, M. Gauding, J. Göbbert, B. Liao, J. Jitsev, H. Pitsch, Towards prediction of turbulent flows at high reynolds numbers using high performance computing data and deep learning, *Lecture Notes in Computer Science* 11203 (2018) 614–623.

[10] P. Srinivasan, L. Guastoni, H. Azizpour, P. Schlatter, R. Vinuesa, Pre-

dictions of turbulent shear flows using deep neural networks, *Physical Review Fluids* 4 (5) (2019) 054603.

[11] C. J. Lapeyre, A. Misdariis, N. Cazard, D. Veynante, T. Poinso, Training convolutional neural networks to estimate turbulent sub-grid scale reaction rates, *Combustion and Flame* 203 (2019) 255–264.

[12] K. Fukami, Y. Nabae, K. Kawai, K. Fukagata, Synthetic turbulent inflow generator using machine learning, *Physical Review Fluids* 4 (6) (2019) 064603.

[13] M. Bode, N. Collier, F. Bisetti, H. Pitsch, Adaptive chemistry lookup tables for combustion simulations using optimal b-spline interpolants, *Combustion Theory and Modelling* 23 (4) (2019) 674–699.

[14] G. D’Alessio, A. Parente, A. Stagni, A. Cuoci, Adaptive chemistry via pre-partitioning of composition space and mechanism reduction, *Combustion and Flame* 211 (2020) 68–82.

[15] M. Raissi, P. Perdikaris, G. Karniadakis, Physics-informed neural networks: A deep learning framework for solving forward and inverse prob-

- lems involving nonlinear partial differential equations, *Journal of Computational Physics* 378 (2019) 686–707.
- [16] J. Kutz, Deep learning in fluid dynamics, *Journal of Fluid Mechanics* 814 (2017) 1–4.
- [17] M. Bode, M. Gauding, K. Kleinheinz, H. Pitsch, Deep learning at scale for subgrid modeling in turbulent flows: regression and reconstruction, *LNCS 11887* (2019) 541–560.
- [18] M. Bode, M. Gauding, Z. Lian, D. Denker, M. Davidovic, K. Kleinheinz, et al., Using physics-informed enhanced super-resolution generative adversarial networks for subfilter modeling in turbulent reactive flows, *Proceedings of the Combustion Institute* 38 (2021) 2617–2625.
- [19] M. Bode, Applying physics-informed enhanced super-resolution generative adversarial networks to direct numerical simulation data of spray and comparison to classical flamelet models, *arXiv preprint* (2022).
- [20] X. Wang, K. Yu, S. Wu, J. Gu, Y. Liu, C. Dong, Y. Qiao, C. Change Loy, Esrgan: Enhanced super-resolution generative adversarial networks, in: *Proceedings of the European Conference on Computer Vision (ECCV)*, 2018.
- [21] M. Gauding, M. Bode, Using physics-informed enhanced super-resolution generative adversarial networks to reconstruct mixture fraction statistics of turbulent jet flows, in: H. Jagode, H. Anzt, H. Ltaief, P. Luszczek (Eds.), *High Performance Computing*, Vol. 11203, Springer International Publishing, 2021, pp. 138–153.
- [22] M. Bode, AI super-resolution: Application to turbulence and combustion, in: N. Swaminathan, A. Parente (Eds.), *Machine Learning and Its Application to Reacting Flows*, Springer, 2022.
- [23] M. Bode, Applying physics-informed enhanced super-resolution generative adversarial networks to large-eddy simulations of ECN Spray C, *SAE Technical Paper 2022-01-0503* (2022).
- [24] R. Lückerrath, O. Lammel, M. Stöhr, I. Boxx, U. Stopper, W. Meier, B. Janus, B. Wegner, Experimental investigations of flame stabilization of a gas turbine combustor, in: *ASME 2011 Turbo Expo: Turbine Technical Conference and Exposition*, American Society of Mechanical Engineers, 2011, pp. 725–736.
- [25] G. P. Smith, D. M. Golden, M. Frenklach, N. W. Moriarty, B. Eiteneer, M. Goldenberg, C. T. Bowman, R. K. Hanson, S. Song, G. William C., V. V. Lissianski, Z. Qin, *GRI-Mech*.
- [26] S. Luca, A. N. Al-Khateeb, A. Attili, F. Bisetti, Comprehensive Validation of Skeletal Mechanism for Turbulent Premixed Methane–Air Flame Simulations, *Journal of Propulsion and Power* (2017) 1–8.
- [27] A. L. Maas, A. Y. Hannun, A. Y. Ng, Rectifier nonlinearities improve neural network acoustic models, *Proceedings of the 30th International Conference on Machine Learning* 30 (2013).
- [28] A. Krizhevsky, I. Sutskever, G. E. Hinton, Imagenet classification with deep convolutional neural networks, in: *Advances in neural information processing systems*, 2012, pp. 1097–1105.
- [29] J. Hirschfelder, C. Curtiss, R. Bird, M. Mayer, *Molecular theory of gases and liquids*, 1964.
- [30] M. Bode, Applying physics-informed enhanced super-resolution generative adversarial networks to turbulent non-premixed combustion on non-uniform meshes and demonstration of an accelerated simulation workflow, *arXiv preprint* (2022).
- [31] F. Hutter, L. Kotthoff, J. Vanschoren (Eds.), *Automated Machine Learning - Methods, Systems, Challenges*, Springer, 2019.
- [32] M. Bode, M. Gauding, D. Goeb, T. Falkenstein, H. Pitsch, Applying physics-informed enhanced super-resolution generative adversarial networks to turbulent premixed combustion and engine-like flame kernel direct numerical simulation data, *arXiv preprint* (2022).